RSC Advances

ROYAL SOCIETY OF CHEMISTRY

www.rsc.org/advances

RSC Advances

ARTICLE

Adsorption of perrhenate ion by bio-char produced from *Acidosasa edulis* shoot shell in aqueous solution

Hui Hu*, Bangqiang Jiang, Jubin Zhang, Xiaohui Chen

-+
Received 00th January 20xx,
Accepted 00th January 20xx

DOI: 10.1039/x0xx00000x

www.rsc.org/

Perrhenate ions adsorption by the bio-char prepared from *Acidosasa edulis* shoot shell at 773K was investigated under acidic conditions. The effects of some important parameters including initial pH (1.0–6.0), adsorbent dose (0.8–8.0 $g \cdot L^{-1}$), contact time (2–480 min) and initial perrhenate ions concentration (10–100 $mg \cdot L^{-1}$) were tested on the recovery of perrhenate ions from aqueous solution in batch experiments. The adsorbent was characterized by Scanning Electron Microscopy equipped with an energy-dispersive X-ray spectroscopy (SEM-EDX), Attenuated Total Reflection Fourier Transform Infrared Spectroscopy (ATR-FTIR) and specific surface area analysis. The adsorption data were well described by Freundlich isotherm and maximum perrhenate ions adsorption capacities of 14.6 $mg \cdot g^{-1}$ for *Acidosasa edulis* shoot shell bio-char under the optimum conditions. Kinetics of adsorption was found to follow the pseudo-second-order rate equation. Thermodynamic analysis suggested that the adsorption was an endothermic process and occur spontaneously. FTIR analysis confirmed a major involvement of the participation of hydroxyl and carboxyl groups during perrhenate ions adsorption. Further more than 94% of total rhenium adsorbed could be recovered using 0.1 $mol \cdot L^{-1}$ KOH as desorption medium. The mechanism analysis indicated that the outer-sphere complexes and electronic attraction mechanism were involved in the adsorption of perrhenate ions. Results from this study indicated that AESS waste derived bio-char can act as an effective adsorbent material for perrhenate ions recovery from copper smelting acidic wastewater.

1. Introduction

Rhenium (Re) is an important rare disperse metal, the average abundance of rhenium less than one part per billion in the earth's crust [1]. According to statistics, identified rhenium resources are estimated to be about only 2500 ton in the world [2]. Considering the declining resource of rhenium against the increasing demand, efforts should be made for searching the new sources of rhenium.

Copper concentrate, which is the raw materials of copper smelting industry, contains trace amount of rhenium. In pyrometallurgical processing of copper concentrates, more than 80% of rhenium is distributed in copper smelting acidic wastewater in the form of $HReO_4$ [3]. And copper smelting acidic wastewater has the characteristics of high acidity (pH value ~1) and low rhenium concentration (~10 $mg \cdot L^{-1}$). At present, solvent extraction [4], ion exchange [5] and chemical precipitation [6] are major methods that have been applied to recover rhenium from copper smelting acidic wastewater. However, these methods have their own inherent limitations such as the complexity of technological process, secondary pollution, high energy requirements and high cost in the processing of low concentration rhenium recovery. Adsorption, as a promising technique, has been proved to be a simple and economical technology for metals recovery [7, 8]. Various adsorbents have been developed and used for perrhenate ions recovery, including persimmon residua [9], orange peel [10], brown algae [11] and impregnated resin [12]. However, some of these adsorbents have low adsorption capacities or have difficulty for regeneration and reuse. Therefore, it is necessary to develop an adsorbent with high adsorption capacity, high-efficiency and environment-friendly that can be applied to recover rhenium from copper smelting acidic wastewater.

Bio-char is a pyrogenic carbon material produced by combustion of biomass, such as wood, dairy manure under oxygen limited and at relatively low temperatures (<973 K) conditions [13-16]. Now, bio-char has been widely applied in soil improvement [17], fertility enhancement [18] and carbon sequestration [19]. Moreover, Bio-char, due to its large specific surface area, porous structure, enriched surface functional groups and mineral components, makes it possible to be used as a potential adsorbent with high adsorption capacity to recover metal ions of low concentration from aqueous solutions [20]. The conversion of agricultural and forest residues into bio-char by biomass carbonization technology to dispose sewage and recover metal ions is a new resource utilization technology of agricultural and forest residues in recent years.

Acidosasa edulis is cultivated in Fujian province of China, and the shoot output is approximately 20 tons per hectare. *Acidosasa edulis* shoot shell (AESS), a by-product of the bamboo shoot processing industry, is an abundant and renewable agricultural residue. However, they are usually eliminated by either burning or discarding in the fields, causing severe environment contamination.

Correspondence to: Hui Hu, School of Chemical Engineering, Fuzhou University, Fuzhou, 350116, China. E-mail: huhui@fzu.edu.cn.
†Electronic Supplementary Information (ESI) available. See DOI: 10.1039/x0xx00000x

The investigation of the *Acidosasa edulis* shoot shell as adsorbent to recover copper ions from sewage has been completed in our previous paper [21]. The results showed that AESS could be used as an effective and low-cost biosorbent for Cu^{2+} removal from aqueous solutions, but its adsorption capacity is not strong enough. Similar results were also reported in the study of copper adsorption by *Freely Suspended Sargassum* [22], *Exhausted Coffee* [23] and *Pretreated Aspergillus Niger* [24]. In order to solve this problem, *Acidosasa edulis* shoot shell was prepared to *Acidosasa edulis* shoot shell bio-char (ASBC) as a potential adsorbent for the recovery of perrhenate ions in this paper. Until now, there are no reports on such usage of bio-char as an adsorbent for the recovery of rhenium.

The main objective of this study was to investigate the adsorption ability of Re (*VII*) by ASBC in aqueous solution. In this study, bio-char was characterized by Scanning Electron Microscopy equipped with an X-ray detector (SEM-EDX), Attenuated total Reflection Fourier Transform Infrared Spectroscopy (ATR-FTIR) and Brunauer–Emmett–Teller (BET) analysis. Batch experiments were used to study the adsorption of Re (*VII*) by ASBC. In addition, the kinetics and isotherms of rhenium adsorption onto ASBC were investigated to understand the underlying mechanism and the thermodynamic functions variations (ΔH^0, ΔS^0, and ΔG^0) are evaluated and discussed.

2. Materials and methods

2.1 Bio-char preparation

Acidosasa edulis shoot shell was collected from a market in Minhou County, Fujian Province, PR China. Firstly, the collected materials were washed several times with tap water and after this with distilled water to clean the adhering dirt. Secondly, the washed materials were dried in the oven at 333 K for more than 48h. Then the dried AESS was ground and sieved through a 180μm sieve. Finally, the resulting product was stored in airtight container for later use.

The method of bio-char preparation could be described as follows [25]. The ground AESS was placed in a ceramic crucible with a lid and pyrolyzed in a muffle furnace under oxygen-limited condition. Feedstock was carbonized at the peak temperature of 773 K for 1 h. The resulting sample was cooled to room temperature inside the furnace and then washed with distilled water to neutral. The residue was dried at 353 K for 24 h to removal the moisture. The obtained bio-char was stored in desiccators for the following experiments.

2.2 Bio-char characterization

The pore structure characteristics of the resulting bio-char were determined by nitrogen adsorption at 77 K using an automatic adsorption instrument with ± 0.15% accuracy (ASAP2020M+C, USA). Prior to gas adsorption measurements, the samples were degassed at 523 K in a vacuum condition for 6h. Adsorption data were obtained over a relative pressure, P/P_0, ranging from approximately 10^{-5} to 1. The specific surface area of ASBC was measured by using the Brunauer–Emmett–Teller (BET) nitrogen adsorption isotherm method. The total pore volumes (V_t, $m^3 \cdot g^{-1}$) were estimated to be the liquid volumes of N_2 at a high relative pressure near unity (~0.99).

The surface morphology of the ASBC before and after adsorption was analyzed by a scanning electron microscopy (HIROX SH-4000M). EDX analyses were conducted by using X-Flash Six Model Energy Dispersive X-ray Microanalysis System (Bruker Corporation, USA) attached to SEM. Accelerating voltage was kept constant at 20 kV, to facilitate the emission of secondary X-rays.

Attenuated total reflection Fourier transform infrared spectroscopy (Thermo Nicolet iS50 ATR-FTIR, USA) was used to determine both active groups and changes in vibrational frequencies in the functional groups of the ASBC and ASBC loaded with rhenium. The spectra were obtained within the wavenumber range of 4000-400 cm^{-1} with a 4 cm^{-1} resolution. The influence of atmospheric water and CO_2 was always subtracted. The baseline of the raw data was adjusted and then the modified data were normalized, by OMNIC 8.2.0.387 software (Thermo Scientific, USA). Before FTIR analysis, the samples were dried in an oven at 333K for 24 h.

Bio-char surface acid functional group distribution was determined using the Boehm titration method [21]. First of all, 50 mL of 0.05 $mol \cdot L^{-1}$ titrating solution and 0.2 g of ASBC were added to a 100mL conical flask. Then the flask was immersed in a constant-temperature water bath set at 298 K for 5 days. And the flask was agitated manually three times a day. Afterwards, a sample of 10mL was collected and 20 mL of 0.05 $mol \cdot L^{-1}$ hydrochloric acid was added, finally all solutions were titrated with 0.05 $mol \cdot L^{-1}$ NaOH solution with phenolphthalein as indicator. The titration was carried out in triplicates.

Procedure for determination of the point of zero charge (pH_{pzc}) [26]: To a series of 20-mL glass vials, 10mL 0.01 $mol \cdot L^{-1}$ of NaCl aqueous solution was transferred in each vial. The pH_i values of the solution were roughly adjusted from 2 to 12 by adding either 0.1 $mol \cdot L^{-1}$ HCl or 0.1 $mol \cdot L^{-1}$ NaOH. The pH_i values of the solutions were then accurately noted. 0.1 g of ASBC was added to each vial, which were securely capped immediately. The suspensions were then shaken in an orbital shaker and allowed to equilibrate for 48 h. The pH values of the supernatant liquid were noted. The difference between the final pH (pH_f) and initial pH_i values ($\Delta pH = pH_f - pH_i$) was plotted against the pH_i. The point of intersection of the resulting curve at which ΔpH 0 gave the pH_{pzc}.

The pH value of ASBC was measured in deionized water at the ratio of 1:20 w/v after being shaken for 24 h at 160 rpm (SHA-B, China).

2.3 Solution preparation

A stock solution containing 1$g \cdot L^{-1}$ Re (*VII*) was prepared by dissolving 0.1554 g analytical grade $KReO_4$ in 100 mL deionized water. Then a series of Re (*VII*) solutions with various concentrations (20, 40, 60, 80, and 100 $mg \cdot L^{-1}$) were prepared by successive dilution. All the experimental solutions were prepared by diluting the stock solution with deionized water. And the solution pH was adjusted by the addition of 0.1 $mol \cdot L^{-1}$ HCl or 0.1 $mol \cdot L^{-1}$ NaOH.

2.4 Batch adsorption studies

The adsorption experiments of Re (*VII*) on ASBC were performed by using a batch equilibration technique. Each experiment was conducted on orbital shaker at 160 rpm for 8 h at 298 K in 20-mL glass vial containing 10 mL of adsorbate solution at optimum pH (pH=1). After agitation the contents of the vials were filtered. The Re (*VII*) concentration in the filtrate was subsequently determined by UV Spectrophotometer.

The effect of solution adsorbent dose (range 0.8–8.0 g·L^{-1}), contact time (2–480 min), pH (1.0–6.0) and temperature (298, 303 and 308K) on the adsorption rate and capacity were studied.

The test of adsorbent dosage effect was carried out at different concentrations in the range of 0.8 to 8.0 g·L^{-1} with the initial adsorbate solution pH=1 and suspensions were shaken at 298 K for 480 min.

The optimum contact time was determined by varying the contact time in the range of 2–480 min at a constant adsorbent dosage (3 g·L^{-1}) and temperature (298 K) for 480 min.

The effect of pH on adsorption of Re (VII) by ASBC was investigated: 10 mL of 20 mg·L^{-1} $KReO_4$ with different pH (1.0–6.0) was placed in 20-mL empty glass vials and 0.03 g of ASBC then added to each vial.

For adsorption isotherms, a series of 20-mL glass vials were filled with 10 mL Re(*VII*) solution of varying concentrations (20–100 mg·L^{-1}), maintained at the desired pH (pH=1) and adsorbent dosage (3 g·L^{-1}). Then an equal amount of ASBC was added into each glass vial. After the optimum uptake time (480 min) the concentrations of rhenium ions were calculated by taking the difference in their initial and final concentrations. The experiments were repeated at 298, 303 and 308 K, respectively.

To obtain adsorption kinetic data, the adsorbent (3 g·L^{-1}) was suspended in rhenium solutions (20 mg·L^{-1}) at three different temperatures i.e. 298, 303 and 308 K wherein the extent of adsorption was analyzed at regular time interval.

The amount of Re (*VII*) adsorbed per unit mass of the adsorbent was evaluated by using the following mass balance equation,

$$q_t = \frac{(C_0 - C_t)V}{W} \quad (1)$$

where q_t (mg·g^{-1}) is the adsorption capacity of the adsorbent. Initial, final concentrations of the metal ions are denoted by C_0, C_t, respectively. *W* is the mass of the adsorbent (g) taken in V volume of solution (L).

The percent recovery of Re (VII) was calculated as follows:

$$\%\ \text{Recovery of}\ Re(VII) = \frac{C_i - C_f}{C_i} \times 100 \quad (2)$$

where C_i is the initial concentration of adsorbate and C_f stands for the final concentration measured after adsorption.

2.5 Regeneration and reuse of adsorbent

In order to determine the reusability of the adsorbent, consecutive adsorption–desorption cycles (Fig.S1) were repeated three times. For this, 0.1mol·L^{-1} KOH, was used as the desorbing agent.

In each cycle, the ASBC was loaded with rhenium ions by adding 0.03 g of dried ASBC to 10 mL of metal solution with a constant concentration of 20 mg·L^{-1} at pH value of 1 at 303 K. The suspension was shaken for 8 h at a speed of 160 rpm. Then the ASBC loaded with rhenium was placed in the desorbing medium and was constantly stirred on a rotatory shaker at 160 rpm for 24 h at 303 K. After each cycle of adsorption and desorption, the ASBC biomass was filtered and the filtrate was used to determine the Re (*VII*) concentration and reconditioned for adsorption in the succeeding cycle. The desorption performance was determined as follows:

$$\varepsilon = \frac{C_2 V_2}{(C_0 - C_1)V_1} \times 100\% \quad (3)$$

where ε is the desorption performance, C_0, C_1 and C_2 are the initial, adsorption and desorption equilibrium concentration of Re(*VII*); V_1,V_2 stands for the volume of adsorption and desorption, respectively.

2.6 Adsorption models

2.6.1 Kinetic models

For fitting of kinetic data, the models of pseudo-first-order [27], pseudo-second-order [28], Elovich [29] and Intra-particle diffusion [30]were used. The linear equations are given as follows:

a. Pseudo-first-order model (PFO)

$$\log(q_e - q_t) = \log q_e - \frac{k_1}{2.303} t \quad (4)$$

b. Pseudo-second-order model (PSO)

$$\frac{t}{q_t} = \frac{1}{k_2 q_e^2} + \frac{1}{q_e} t \quad (5)$$

$$h = k_2 q_e^2 \quad (6)$$

c. Elovich model

$$q_t = \frac{1}{\beta}\ln(\alpha\beta) + \frac{1}{\beta}\ln t \quad (7)$$

d. Intra-particle model (IPD)

$$q_t = k_p t^{0.5} + C \quad (8)$$

where q_t and q_e are the amount of metal ion adsorbed at any given time (*t*) and at equilibrium (mg·g^{-1}), respectively. k_1 (min^{-1}) is the rate constant for pseudo-first-order model. k_2 (g·mg^{-1}·min^{-1}) is the rate constant for pseudo-second-order. *h* (mg·g^{-1}·min^{-1}) is the initial adsorption rate at t = 0. α (mg·g^{-1}·min^{-1}) is the initial sorption rate constant, and β (g·mg^{-1}) is related to the extent of surface coverage and activation energy for chemisorption. k_p (mg·g^{-1}·min$^{-0.5}$) is the intra-particle diffusion rate constant.

Pseudo-first order kinetic model was based on the assumption of physic-sorption process [31], while pseudo-second order model was based on the assumption that the rate-limiting step may be chemical sorption involving valency forces through sharing or exchange of electrons between the adsorbent and adsorbate [28]. The Elovich equation is a valuable tool to examine any changes of surface reactivity in the adsorbent during the whole course of reaction time. Any changes of the reactivity of sorption sites on surface should be reflected in breaks of the Elovich linear plot [29]. It has been used not only for describing reactions involving chemisorption of gases on a solid surface, but also for simulating sorption kinetics in a liquid phase [32]. The intra-particle diffusion model is used to determine the rate limiting step of the adsorption

kinetics. When the intra-particle mass transfer resistance is the rate limiting step, then the sorption process is described as being particle diffusion controlled. If the plot of q_t versus $t^{0.5}$ satisfies the linear relationship and passes through the origin, then the sorption process is controlled by intra-particle diffusion only. But, if the data exhibit multi-linear plots, then sorption process may influenced by two or more steps [21, 29].

2.6.2 Isotherm models

Adsorption isotherms are mainly used to describe how adsorbate ions or molecules interact with adsorbent surface sites and its degree of accumulation onto adsorbent surface at a constant temperature. In this study, three two-parameter isotherm equations, namely, Langmuir [33], Freundlich [34], Temkin [35] have been used to fit the experimental data. The equations are given as follows:

a. Langmuir isotherm model

$$q_e = \frac{q_{max} K_L C_e}{1 + K_L C_e} \quad (9)$$

b. Freundlich isotherm model

$$q_e = K_f C_e^{1/n} \quad (10)$$

c. Temkin isotherm model

$$q_e = \frac{RT}{b} \ln\left(A C_e\right) \quad (11)$$

where C_e is the equilibrium concentration of adsobate (mg·L^{-1}), q_e is the equilibrium amount of metal adsorbed on ASBC (mg·g^{-1}), q_{max} is the maximum loading capacity of ASBC (mg·g^{-1}), K_L is the Langmuir isotherm constant related to the energy of adsorption (L·mg^{-1}), K_f is the Freundlich isotherm constant related to the adsorption capacity ((mg$^{1-(1/n)}$·L$^{1/n}$·g^{-1}), *1/n* is the heterogeneity factor, *A* is a Temkin isotherm equilibrium binding constant which takes into account the interactions between the adsorbate and the adsorbent (L·mg^{-1}), *R* is the universal gas constant (8.314 J·mol^{-1}·K^{-1}), *b* is Temkin isotherm constant related to heat of adsorption (J·mol^{-1}), *T* is the absolute temperature (K) and *M* is the molar mass of metal ions.

The Langmuir isotherm model describes quantitatively about the formation of a monolayer adsorbate on the outer surface of the adsorbent and after that no further adsorption takes place. In addition, Langmuir represents the equilibrium distribution of adsorbate between the solid and liquid phases [36]. The Freundlich isotherm equation is an empirical equation used for the description of multilayer adsorption with interaction between adsorbed molecules, and it is widely used to describe adsorption onto a heterogeneous surface and a multilayer sorption occurs on the surface. [34]. The Temkin isotherm based on the assumption that the decline of the heat of sorption as a function of temperature is linear rather than logarithmic [37].

2.6.3 Thermodynamic models

To describe thermodynamic behavior of the adsorption of Re (*VII*) onto ASBC, thermodynamic parameters such as Gibbs free energy change (ΔG^0), enthalpy change (ΔH^0) and entropy change (ΔS^0) for the adsorption systems were calculated by using the following equations:

$$\Delta G^0 = -\mathrm{RT} \ln\left(K^0\right) \quad (12)$$

$$\Delta G^0 = \Delta H^0 - T \Delta S^0 \quad (13)$$

$$\ln K^0 = \frac{\Delta S^0}{R} - \frac{\Delta H^0}{R} \frac{1}{T} \quad (14)$$

where *R* is the gas constant (8.314 J·(mol·K)$^{-1}$), *T* is the absolute temperature (K), K^0 is Langmuir constant. ΔG^0 is the standard free energy change of the ion exchange (kJ·mol^{-1}), ΔH^0 is the enthalpy (kJ·mol^{-1}), ΔS^0 is the entropy (J·mol^{-1}·K^{-1}).

3. Results and discussion

3.1 Characterization of ASBC

3.1.1 Physico-chemical characteristics

The physico-chemical characteristics of the ASBC used in this experiment are shown in Table S1. The pH values of the ASBC is alkaline, which may be influenced by two factors as follows: (i) organic function groups and (ii) inorganic alkalis [38]. ASBC had the higher specific surface area (6.368 m^2·g^{-1}), compared to peanut shell derived bio-char (5.06 m^2·g^{-1}) at the same temperature [39], which may contribute to the Re (*VII*) adsorption. The pHpzc was used to assess the surface properties of the ASBC adsorbent. An adsorbent surface is positively charged at pH < pHpzc and is negatively charged at pH > pHpzc. The pHpzc of the ASBC adsorbent was found to be 7.74 (Table S1). Thus, ASBC surfaces are become positively charged in acidic solution, which will help to perrhenate anion adsorption on ASBC.

Table S2 compiles the results of surface acidic functional groups of ASBC detected by the method of Boehm titration. These polar functional groups may form active sites for adsorption on the material surface. Results of active sites determination on ASBC reveal that it contains 0.0381mmol·g^{-1} of carboxylic group, 0.0193mmol·g^{-1} of lactone group, 0.3941mmol·g^{-1} of phenolic group and a total acidity 0.4515 mmol·g^{-1}. These acidic function groups could transform into –COOH^{2+}, –OH^{2+} or =C=OH$^+$ by reaction with H$^+$ in the solution. The more that these cations existed on the ASBC surface, the better the recovery of perrhenate anion via adsorption from aqueous solution. The predominant acid group in ASBC is the phenolic group and carboxylic group comes second, both of them are contributed to the Re (*VII*) adsorption on ASBC.

3.1.2 SEM-EDX analysis

The SEM analysis of ASBC reveals important information on the surface morphology (Fig.1). Fig.1 clearly demonstrates porous and rough surfaces with a disorganized structural pattern of ASBC and the pore sizes are inconsistent, which was of importance to liquid-solid adsorption processes [40]. The pores can be attributed to escaping volatiles during high temperature decomposition [41].

RSC Advances

ARTICLE

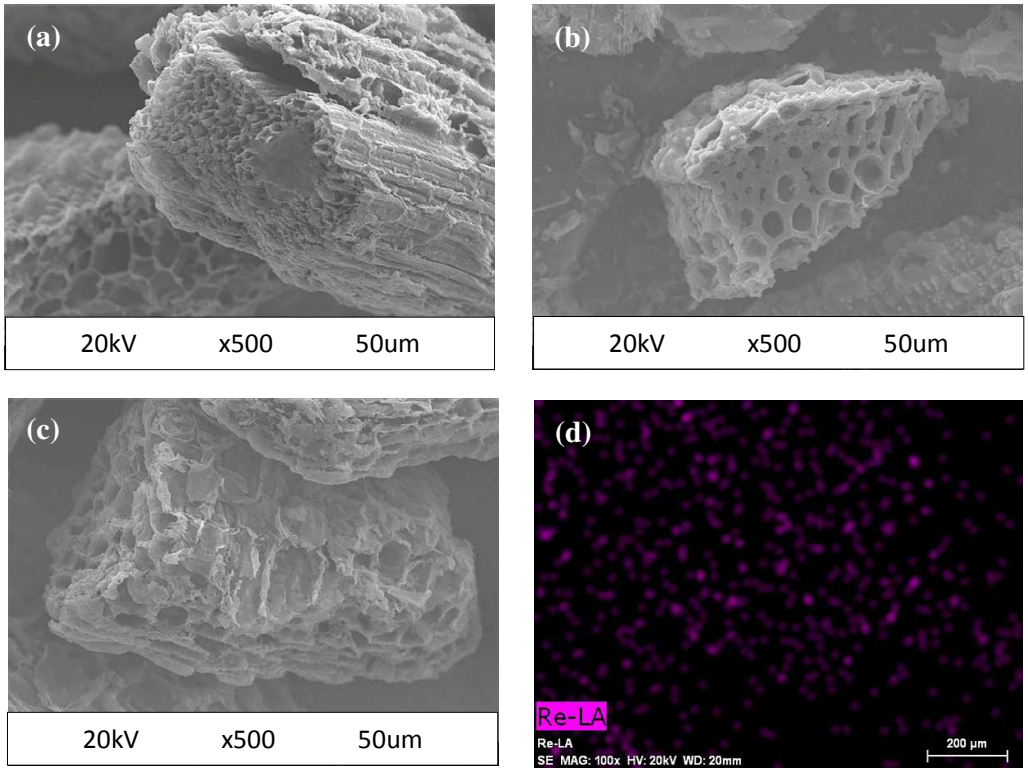

Fig. 1. SEM micrograph of (a) (b) ASBC, (c) ASBC-Re and (d) X-ray elemental mapping.

In the present study, Energy Dispersive X-ray analysis of the raw as well as rhenium adsorbed adsorbents viz. ASBC was performed in order to study the surface changes of the elements. As shown in Fig. S2, carbon and oxygen are the main constituents of ASBC. Apart from that nitrogen, potassium, silicon and sodium are also present in low proportion. In the EDX spectrum of ASBC after Re (*VII*) adsorption, a new peak of Re (*VII*) emerged, which confirmed that the rhenium was adsorbed onto it. Furthermore, the Re elemental mapping shows the presence of rhenium onto bio-char in irregular ways. That irregular contribution of rhenium loaded onto bio-char surface indicates their heterogeneous structure.

3.1.3 FT-IR analysis

The FTIR spectrum is carried out as a qualitative analysis to investigate the main functional groups that are involved in the adsorption process. Fig.2 showed the ATR-FTIR spectra of ASBC before and after adsorption of Re (*VII*). In the case of ASBC, the spectra display several vibrational bands indicating the complex nature of the materials. As shown in Fig.2, the absorption peak around 3340 cm^{-1} can be assigned to O–H stretching vibration [14]. Peak at 1700 cm^{-1} is C=O stretching vibration of carboxyl groups. The peak at 1571 cm^{-1} can be assigned to C=C stretching vibration of aromatic rings [42] . Bands at 1061 and 1359 cm^{-1} may indicated the stretching vibration of O-H and C-O stretching vibration of carboxylic groups [14]. The band observed at 881 and 749 cm^{-1} was assigned to C-H stretching vibration of aromatic compounds [39].

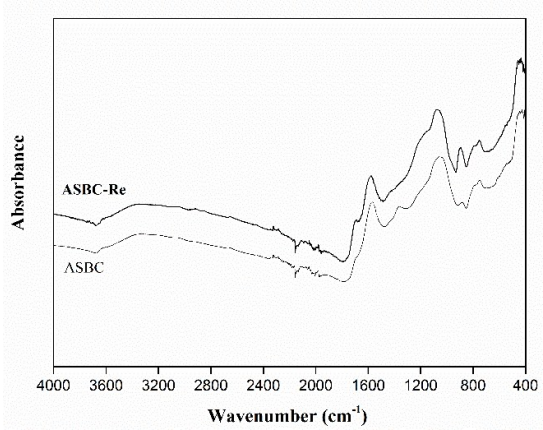

Fig. 2. ATR-FTIR spectra for ASBC (a) and (b) after perrhenate adsorption.

Compared with the spectra of ASBC, the intensity of the O–H stretching peak of the ASBC at the region of 3340 cm^{-1} has been found to be increased after adsorption, which indicated significant hydrogen-bonding interactions in acidic conditions. A new band close to 1700 cm^{-1} have been appeared after ASBC loaded with rhenium, the peaks around 1359 cm^{-1} have been diminished and 1061 cm^{-1} have been increased, indicating that carboxyl groups took part in the adsorption process. That the intensities of bands at 881, 749 cm^{-1} gradually enhanced indicates the increase of aromatic fractions and the enhancement of carbonization degree [43].

3.2 Effect of solution pH

Earlier researches on metal adsorption have indicated that pH was quite important single parameter affecting the adsorption process [44-46]. The plot of Re (*VII*) adsorption capacity versus pH is shown in Fig.3. As seen from the figure, a sharp increase is observed at pH less than 2.0, it is shown that the ASBC has a high affinity for Re (*VII*) at high acid concentration, and when pH>2.0, the adsorption capacity decreased significantly. These phenomena can be explained as follows.

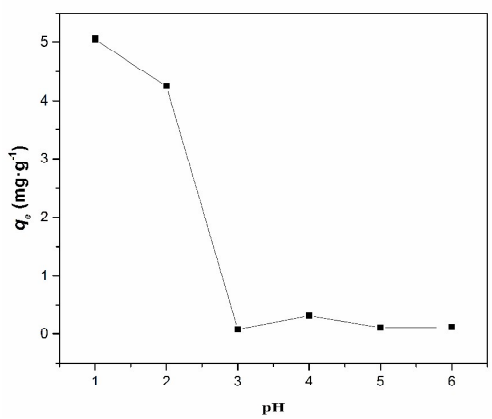

Fig. 3. Effect of pH on Re (*VII*) adsorption on ASBC. Conditions: adsorbent dosage, 3 g·L^{-1}; initial Re (*VII*) concentration, 20 mg·L^{-1}; contact time, 480 min; temp., 298K.

In aqueous phase, rhenium is stable, and its dominant species being the perrhenate anion (ReO_4^-) [47]. The behavior for better adsorption at low pH by ASBC may be attributed to the large numbers of H^+ ions present at low pH values which protonate the ASBC surface (Eq. (15-16)). That results in strong electrostatic attraction between positively charged adsorbent surface and ReO_4^- leading to higher adsorption. The adsorption mechanism can be expressed as Eq. (15-18), which has been confirmed by FTIR spectra and thermodynamic analyses. As the pH of the system increases, the number of negatively charged sites increases. A negatively charged surface site on these adsorbents does not favor the adsorption of Re (*VII*) due to the electrostatic repulsion [48]. This explains the decrease in the adsorption of Re (*VII*) ions at higher pH values. Therefore, all the other experiments in this study were carried out at optimum initial pH of 1.0 so as to achieve maximum metal adsorption capacity.

$$X-OH+H^+ \longleftrightarrow X-OH_2^+ \quad (15)$$

$$X-COOH+H^+ \longleftrightarrow X-COOH_2^+ \quad (16)$$

$$X-OH_2^+ + ReO_4^- \longleftrightarrow X-OH_2^+ \ldots ReO_4^- \quad (17)$$

$$X-COOH_2^+ + ReO_4^- \longleftrightarrow X-COOH_2^+ \ldots ReO_4^- \quad (18)$$

It was noticed that the pH of the solution after adsorption slightly increased, which was mainly attributed to that: (i) the H^+ participate in the functional groups protonation (Eq. (15-16)); (ii) H^+ was neutralised by alkaline ASBC; and (iii) affected by the mineral ash from pyrolysis [38].

3.3 Effect of adsorbent dosage contact time

The amount of adsorbent is an important factor to enable the metal adsorption process effectively, and determine the adsorbent–adsorbate equilibrium of the system [49]. In order to determine the effect of the ASBC dose on Re (*VII*) adsorption, ASBC dosage in the range of 0.8–8.0 g·L^{-1} was subjected to adsorption experiments and the results are given in Fig.4.

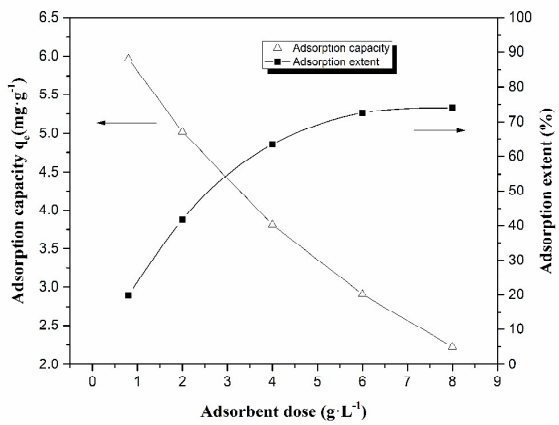

Fig. 4. Effect of adsorbent dosage on the uptake of Re (*VII*) onto ASBC. Conditions: initial Re (*VII*) concentration, 20 mg·L^{-1}; pH, 1.0; temperature, 298K.

As Fig.4 shows, the adsorption amount decreases with an increase in adsorbent dose. On the other hand, the extent of the adsorption increased first with an increasing amount of adsorbent and almost constant at dose higher than 6 g·L^{-1}, that is, adsorption reached saturation. This results could be explained as a consequence of partial aggregation of ASBC at higher concentration, which leads to the decrease in effective surface area for adsorption [50]. Thus, it is reasonable to choose adsorbent dosage 3 g·L^{-1} for all further experiments to ensure higher adsorption capacity and adsorption rate.

3.4 Effect of contact time

The results of effect of contact time on ASBC adsorption of Re (*VII*) are shown in Fig.5. It is apparent that increase in contact time from 2 to 120 min enhanced the amount adsorption of Re (*VII*) considerably, due to the strong attraction between rhenium ions resulting from a large number of binding sites on the surface of ASBC; then the initial rapid adsorption gives away a very slow approach to equilibrium. There are two reasons for this, on the one hand, due to the binding sites on ASBC surface are being used up, it will take more time to enter the adsorbent interior and combine with the active sites [21]; on the other hand, since active adsorption sites in a determined system have a fixed number and each active

site can adsorb only one metal ion in a monolayer, the metal uptake by the adsorbent surface will be rapid at the beginning, then slowing down as the competition for the decreasing availability of active sites intensifies by the metal ions remaining in the solution [51]. These results shows that a contact time of 480 min will be sufficient for the removal of Re (*VII*) ions by ASBC under the other adsorption conditions determined as optimal in this study.

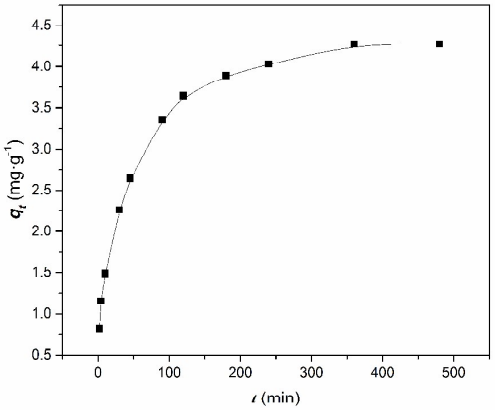

Fig. 5. Effect of contact time on the Re (*VII*) capacity of ASBC. Conditions: adsorbent dosage, 3 g·L^{-1}; initial Re (VII) concentration, 20 mg·L^{-1}; pH, 1.0; temp., 298K.

3.5 Adsorption kinetics

To design and control adsorption process, it is necessary to study the adsorption process rate and dynamic behavior. In general, adsorption on an adsorbent from the aqueous phase involves three steps: (i) the transport of the adsorbate from the bulk phase to the exterior surface of the adsorbent (film diffusion), (ii) the transport into the adsorbent by either pore diffusion and/or surface diffusion (intra-particle diffusion) and (iii) the adsorption on the surface of the adsorbent [52]. The slowest of these steps, that is, the rate-limiting steps determines the overall rate of the adsorption process. Research shows that adsorption kinetics has a strong dependence on the physical and/or chemical characteristics of the bio-char which also influences the sorption mechanism [39, 53].

Adsorption kinetics of Re (*VII*) on the ASBC were studied by monitoring the concentration of metal ions at various temperatures (298, 303 and 308 K). The conformity between experimental data and the model predicted values was expressed by the adjusted correlation/determination coefficients (R_{adj}^2 values close or equal to 1). A relatively high R_{adj}^2 value indicates that the model successfully describes the kinetics of the adsorption.

The parameters of kinetic models were obtained with the linear fitting procedure and listed in Table S4. The appropriate plots of the PSO and IPD kinetic model are shown in Fig.S3. The PFO model did not adequately describe the adsorption results of Re (*VII*) onto the ASBC due to low correlation coefficients between the calculated q_e values and the experimental values. Taking the R^2 values into account, a better fit was achieved when the PSO model was used. The result also reconfirms that the PSO model is suitable to explain the adsorption of low molecular weight compounds on small adsorbent particles [54]. The values of the rate constants (k_2) and initial adsorption rate (h) are varied as the temperature increased from 298 to 308 K, which shows that the adsorption process highly depends on temperature.

As for the Elovich equation (Chemisorption control), the determination coefficient is lower than the PSO equation. This situation indicates that the Elovich equation might not be adequate to describe the adsorption model, since adsorption process may not be controlled by chemisorption completely.

The possibility of application of the intra-particle diffusion process was also evaluated by using the Weber and Morris model (Eq. (8)). In order to establish whether the transport of Re (*VII*) ions from the solution into the pores of the ASBC is the rate controlling step, the relationship between q_e and $t^{1/2}$ was plotted. The intra-particle diffusion plot is shown in Fig.S3 (b). It could be obviously observed that not a straight line was obtained. Therefore, it cannot be considered that the intra-particle diffusion was the controlling step for the adsorption Re (*VII*) onto ASBC. However, it should be noticed that for obtaining the relations on the plots there are three separate parts attributed to the film diffusion, the intra-particle diffusion and the equilibrium stage. In the first stage, the available the available active sites on the external surface of the ASBC are sufficient and the adsorption rate is rapid, which suggests the film diffusion is rate-determining step. However, active sites on the external surface of ASBC are occupied gradually with the lapse of time, the rhenium ions have to traverse farther and deeper into the pores and encounter much larger resistance, which indicates that the intra-particle diffusion is rate-determining step during this period. The third part is attributed to the final equilibrium stage where intra-particle diffusion starts to slow down due to extremely low adsorbate concentrations in the solution. Thus, the adsorption of Re (*VII*) with ASBC adsorbent occurred in more than one stage that can occur simultaneously. The rate of uptake might be limited by size of adsorbate molecule or ion, concentration of the adsorbate and its affinity to the adsorbent, diffusion coefficient of the adsorbate in the bulk phase, the pore size distribution of the adsorbate, and degree of mixing. It was also found that the values of the intra-particle diffusion rate k_2 are smaller than the film diffusion rate k_1 as presented in Table S4. Additionally, the comparison of the intercept (C_2) values, which gives an idea about the boundary layer thickness i.e., the larger the intercept, the greater is the boundary layer effect. All in all, the PSO kinetic model provides the best correlation for all of the adsorption processes than the PFO, Elovich equations and IPD. This suggests that the adsorption system belongs to the second-order equation, based on the assumption that the rate limiting step may be chemical sorption or chemisorption involving valency forces through sharing or exchange of electrons between adsorbate and adsorbent [55, 56].

3.6 Adsorption isotherms

The adsorption isotherm data for Re (*VII*) onto the ASBC has been plotted in Fig.S4 and isotherm constants have been depicted in Table S5. Determination coefficients suggested that the Freundlich model fit the data better than the Langmuir and Temkin model. This results illustrate that it can predict rhenium adsorption equilibrium on ASBC more accurately, and the multilayer sorption of Re (*VII*) mainly occur on heterogeneous surfaces of ASBC. The Langmuir and Temkin equations can also predict the rhenium adsorption

equilibrium on ASBC surface well, but not as well as the Freundlich equation.

The constants K_f and n of Freundlich equation were calculated from Eq. (10), and tabulated in Table S5. According to the study by Febrianto et al.[57], if the value of *n* lays between 1 and 10, the adsorption is favorable. It can be observed that the value of n which between 1 and 10 (Table S5) showed the favorability of adsorption of Re (*VII*) onto ASBC [58]. Besides, the Freundlich constants K_f and *n* also increased with temperature, which indicated the adsorption capacity and intensity growing.

In this study, the values of sorption coefficient K_d (K_d = Q_e/C_e, $L{\cdot}g^{-1}$) (Table S5) at different rhenium concentrations (20, 60 and 100 $mg{\cdot}L^{-1}$) were calculated to compare their sorption capacities. Table S5 showed that with increasing Re (*VII*) concentration, the K_d values for ASBC greatly decreased because Re (*VII*) adsorption on the ASBC was nonlinear. From Fig.S4 we observed that the uptake of rhenium ion increases with the rise in temperature from 298, 303, to 308 K. This result also showed that the adsorption was endothermic in nature. This may be attributed to: (1) diffusion rate of the adsorbate increased with temperature, (2) de-protonation reaction increased with temperature, which made more active sites (hydroxyl, carboxyl) available for Re(*VII*) recovery, (3) the thickness of the boundary layer around the adsorbent decreased with temperature, which made mass transfer resistance decreased [59, 60].

3.7 Thermodynamic studies

The thermodynamic parameters of the adsorption process were calculated by Eq. 12, Eq. 13 and Eq. 14. The results were listed in Table 1. It could be seen that all the ΔG^0 values were negative, which suggested the feasibility of the process and the spontaneous nature of the adsorption. Generally, the ΔG^0 value is in the range of 0 to -20 $kJ{\cdot}mol^{-1}$ indicating physical adsorption and -80 to -400 $kJ{\cdot}mol^{-1}$ chemical adsorption [61]. In this study, the ΔG^0 values are in the range of -26.18 to -28.73 $kJ{\cdot}mol^{-1}$, indicating that rhenium adsorption on ASBC could be a combination of physisorption and chemisorption. The decrease in ΔG^0 with an increase in temperature indicated that the reaction was more favorable at higher temperatures.

Table 1 Thermodynamic parameters for the adsorption of Re (*VII*) onto the ASBC.

Temperature	298K	303K	308K
ΔG^0 ($kJ{\cdot}mol^{-1}$)	-26.18	-27.35	-28.73
ΔH^0 ($kJ{\cdot}mol^{-1}$)		11.85	
ΔS^0 ($J{\cdot}mol^{-1}{\cdot}K^{-1}$)		127.46	

The positive ΔH^0 value suggested the endothermic nature of the adsorption, which is in agreement with the experimental observations. That is to say an input of energy is required to bring about the bond formation on Re (*VII*) ions on ASBC. This is because the bonding is short-ranged and as a result, energy is needed to overcome the repulsive force of attraction as ions bind in a short distance from adsorbent. This is the reason why the optimal temperature was relatively higher (308 K), as external source of heat energy is required for the endothermic reaction to occur [62]. In this study, the ΔH^0 value is 11.85 $kJ{\cdot}mol^{-1}$, indicating that the formation of complex between functional groups and perrhenate ions should be mainly outer-sphere surface complexation (Eq. (19)). Because inner-sphere complexes refers to the perrhenate ions and the functional groups of the adsorbent and the adsorbate forms a direct coordinate-covalent bond with surface functional groups on the variable charge surface, the interaction is strong and slow, while, for outer-sphere complexes, the interaction between the surface functional group is weak and rapid [60, 63].

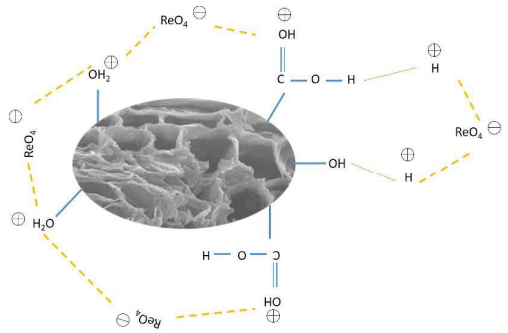

Fig. 6. Conceptual illustration of the affinity between adsorption sites and Re (*VII*).

The positive value of ΔS^0 shows the increased randomness at the solid/solution interface during the adsorption of Re (*VII*) on the ASBC. This indicates strong affinity of the adsorbent for Re (*VII*) ions and there may be some structural changes in both the adsorbate and adsorbent during the adsorption process [62].

3.8 Regeneration and recovery studies

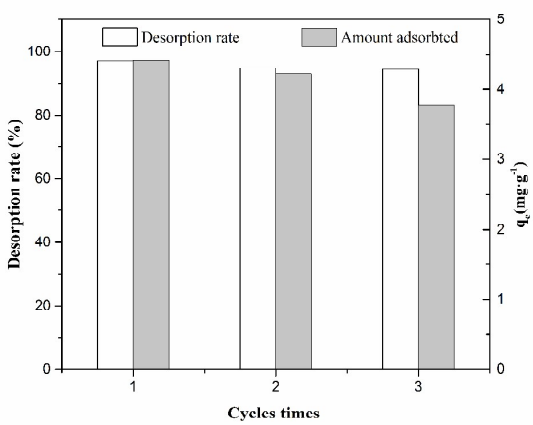

Fig. 7. Reusability of ASBC biomass with repeated adsorption–desorption cycle. Conditions: pH, 1; adsorbent dosage, 3 $g{\cdot}L^{-1}$; initial Re(*VII*) concentration, 20 $mg{\cdot}L^{-1}$; contact time, 480 min; temp., 303K.

The regeneration of the adsorbent is one of the key factors for assessing of its potential for commercial applications. 0.1 $mol{\cdot}L^{-1}$ KOH desorption agent was used to recover the Re (*VII*) ions from the adsorbent. Higher than 94% of the adsorbed Re (*VII*) ions were desorbed from the adsorbent. It is clear that the recovery of rhenium in this study is high, probably because the OH^- ions could easily replace rhenium anions from the adsorbent sites on ASBC. This phenomenon was consistent with the results found by Lou et

al.[47], Shan et al.[10], Xiong et al.[11], indicating the strong affinity between OH^- ions and ASBC.

As shown in Fig.7, the adsorption capacity of ASBC decreased slightly with 0.1 mol·L^{-1} KOH as an eluent after three cycles (from the initial 4.42 mg·g^{-1} to the final 3.78 mg·g^{-1}). This might be attributed to the amount of biomass lost and/or the damages on the surface of the adsorbent due to the continuous contact with the desorbing agent during the adsorption-desorption process. These results indicated that the ASBC biomass could be used repeatedly in Re (*VII*) adsorption studies without any detectable loss in the total adsorption capacity. Therefore, ASBC can be used as a stable adsorbent for Re (*VII*) recovery.

3.9 Comparison of various adsorbents for Re (*VII*) ions adsorption

Table 2 demonstrates a comparison between Re (*VII*) ions adsorption capacity of various type of adsorbents and ASBC. It is clear that the Re (*VII*) ions uptake capacity of ASBC has an encouraging effect in this work. This could probably be due to the number of active groups available for metal ion adsorption and the different sorption mechanisms involved. These results also indicate that ASBC can be used as a high efficiency adsorbent in water treatment to recover rhenium from aqueous solutions.

Table 2 Comparison of maximum adsorption capacities of various adsorbents for Re (*VII*) ions. Conditions: initial Re (VII) concentration, 20 mg·L^{-1}; pH, 1.0.

Adsorbents	Adsorption capacity (mg·g^{-1})	References
Cross-linked persimmon residua (sulfuric acid)	0.10	[9]
Cross-linked astringent persimmon (formaldehyde)	1.30	[64]
La(*III*)-loaded orange peel gels	0.42	[10]
Zr(*VI*)-loaded orange peel gels	0.60	
Cross-linked brown algae (sulfuric acid)	1.01	[11]
Corn stalk	0.9	[61]
ASBC	**5.13**	**Current study**

4. Conclusions

This study investigated the ability of bio-char derived from *Acidosasa edulis* shoot shell to adsorb Re (*VII*) from aqueous solution. The experimental evidence showed the strong effect of the operating variables (adsorbent dosage, contact time, pH value, and temperature) on adsorption performance of ASBC biomass. Adsorption equilibrium is well described by Freundlich adsorption isotherms. Adsorption rate is fast and its kinetic is well represented by pseudo-second-order model. Thermodynamic parameters showed that the adsorption of Re (*VII*) ions onto ASBC was feasible, spontaneous and endothermic under studied conditions. The interactions between the metal ion and the functional groups on the cell wall surface of the biomass were confirmed by FTIR analysis, which indicated the participation of hydroxyl, carboxyl groups in the rhenium adsorption. Taken into consideration of the findings above, it can be stated that the ASBC could be used as an efficient biomass for the treatment of Re (*VII*) containing aqueous solutions.

References

1. P. Voudouris, V. Melfos, P. G. Spry, L. Bindi, R. Moritz, M. Ortelli and T. Kartal, *Minerals*, 2013, **3**, 165-191.
2. S. Jasinski, *US Geological Survey, Department of the Interior, http://minerals. usgs. gov/minerals/pubs/mcs/2015/mcs2015. pdf,(April 29, 2015)*, 2015, 130-131.
3. Z. S. Abisheva and A. Zagorodnyaya, *Hydrometallurgy*, 2002, **63**, 55-63.
4. Z. S. Abisheva, A. N. Zagorodnyaya and N. S. Bekturganov, *Hydrometallurgy*, 2011, **109**, 1-8.
5. C. D. Anderson, P. R. Taylor and C. G. Anderson, *Miner. Metall. Process.*, 2013, **30**, 59-73.
6. H. G. Dong, Y. Liu, X. X. Fan, J. C. Zhao, J. L. Chen, B. J. Li and Y. D. Wu, *Nonferrous Metals (Extractive Metallurgy)*, 2013, 30-33.
7. T. Wang, W. Liu, L. Xiong, N. Xu and J. Ni, *Chem. Eng. J.*, 2013, **215–216**, 366-374.
8. M. Inyang, B. Gao, Y. Yao, Y. Xue, A. R. Zimmerman, P. Pullammanappallil and X. Cao, *Bioresour. Technol.*, 2012, **110**, 50-56.
9. Y. Xiong, C. Chen, X. Gu, B. K. Biswas, W. Shan, Z. Lou, D. Fang and S. Zang, *Bioresour. Technol.*, 2011, **102**, 6857-6862.
10. W. Shan, D. Fang, Z. Zhao, Y. Shuang, L. Ning, Z. Xing and Y.

Xiong, *Biomass & Bioenergy*, 2012, **37**, 289-297.
11. Y. Xiong, J. Xu, W. Shan, Z. Lou, D. Fang, S. Zang and G. Han, *Bioresour. Technol.*, 2013, **127**, 464-472.
12. J. K. Moon, Y. J. Han, C. H. Jung, E. H. Lee and B. C. Lee, *Korean J Chem Eng*, 2006, **23**, 303-308.
13. S. P. Sohi, *Science*, 2012, **338**, 1034-1035.
14. A. Tytak, P. Oleszczuk and R. Dobrowolski, *Environ Sci Pollut R*, 2015, **22**, 5985-5994.
15. X. C. Chen, G. C. Chen, L. G. Chen, Y. X. Chen, J. Lehmann, M. B. McBride and A. G. Hay, *Bioresour. Technol.*, 2011, **102**, 8877-8884.
16. R.-k. Xu, S.-c. Xiao, J.-h. Yuan and A.-z. Zhao, *Bioresour. Technol.*, 2011, **102**, 10293-10298.
17. F. G. A. Verheijen, E. R. Graber, N. Ameloot, A. C. Bastos, S. Sohi and H. Knicker, *Eur J Soil Sci*, 2014, **65**, 22-27.
18. H. Zheng, Z. Wang, X. Deng, S. Herbert and B. Xing, *Geoderma*, 2013, **206**, 32-39.
19. J. Lehmann, *Nature*, 2007, **447**, 143-144.
20. J. C. Yan, L. Han, W. G. Gao, S. Xue and M. F. Chen, *Bioresour. Technol.*, 2015, **175**, 269-274.
21. H. Hu, J. Zhang, K. Lu and Y. Tian, *J. Environ. Chem. Eng.*, 2015, **3**, 357-364.
22. P. X. Sheng, K. H. Wee, Y. P. Ting and J. P. Chen, *Chem. Eng. J.*, 2008, **136**, 156-163.
23. Y. Orhan and H. Büyükgüngör, *Water Science & Technology*, 1993, **28**, 247-255.
24. M. Mukhopadhyay, S. Noronha and G. Suraishkumar, *Bioresour. Technol.*, 2007, **98**, 1781-1787.
25. X. J. Tong, J. Y. Li, J. H. Yuan and R. K. Xu, *Chem. Eng. J.*, 2011, **172**, 828-834.
26. M. Essandoh, B. Kunwar, C. U. Pittman, D. Mohan and T. Mlsna, *Chem. Eng. J.*, 2015, **265**, 219-227.
27. S. Lagergren, *Kungliga Svenska Vetenskapsakademiens. Handlingar*, 1898, **24**, 1-39.
28. Ho, McKay, Wase and Forster, *Adsorpt. Sci. Technol.*, 2000, **18**, 639-650.
29. S. Chien and W. Clayton, *Soil Sci. Soc. Am. J.*, 1980, **44**, 265-268.
30. W. J. Weber and J. C. Morris, *J. Sanit. Eng. Div.*, 1963, **89**, 31-60.
31. B. Singha and S. K. Das, *Colloids and Surfaces B-Biointerfaces*, 2013, **107**, 97-106.
32. I. Alomá, M. A. Martín-Lara, I. L. Rodríguez, G. Blázquez and M. Calero, *Journal of the Taiwan Institute of Chemical Engineers*, 2012, **43**, 275-281.
33. I. Langmuir, *J. Am. Chem. Soc.*, 1916, **38**, 2221-2295.
34. U. Freundlich, *Z. Phys. Chem.*, 1906, **57**, 385-470.
35. M. Temkin and V. Pyzhev, *Acta physiochim. URSS*, 1940, **12**, 217-222.
36. K. R. Hall, L. C. Eagleton, A. Acrivos and T. Vermeulen, *Ind. Eng. Chem. Fundam.*, 1966, **5**, 212-223.
37. S. Basha, Z. Murthy and B. Jha, *Ind. Eng. Chem. Res.*, 2008, **47**, 980-986.
38. J.-H. Yuan, R.-K. Xu and H. Zhang, *Bioresour. Technol.*, 2011, **102**, 3488-3497.
39. Z. Wang, G. Liu, H. Zheng, F. Li, H. H. Ngo, W. Guo, C. Liu, L. Chen and B. Xing, *Bioresour. Technol.*, 2015, **177**, 308-317.
40. D. Mohan, S. Rajput, V. K. Singh, P. H. Steele and C. U. Pittman, *J. Hazard. Mater.*, 2011, **188**, 319-333.
41. R. M. Allen-King, P. Grathwohl and W. P. Ball, *Adv. Water Resour.*, 2002, **25**, 985-1016.
42. J. J. Luo, J. J. Lu, Q. Niu, X. B. Chen, Z. Y. Wang and J. R. Zhang, *Fuel*, 2015, **160**, 440-445.
43. G. Zhang, Q. Zhang, K. Sun, X. Liu, W. Zheng and Y. Zhao, *Environ. Pollut.*, 2011, **159**, 2594-2601.
44. Y. Hannachi, A. Rezgui and T. Boubaker, *Korean J Chem Eng*, 2014, **31**, 1211-1218.
45. G. Mahajan and D. Sud, *Bioresources*, 2011, **6**, 3324-3338.
46. T. Karthikeyan, S. Rajgopal and L. R. Miranda, *J. Hazard. Mater.*, 2005, **124**, 192-199.
47. Z. N. Lou, Z. Y. Zhao, Y. X. Li, W. J. Shan, Y. Xiong, D. W. Fang, S. Yue and S. L. Zang, *Bioresour. Technol.*, 2013, **133**, 546-554.
48. Z. A. Zakaria, M. Suratman, N. Mohammed and W. A. Ahmad, *Desalination*, 2009, **244**, 109-121.
49. A. R. Iftikhar, H. N. Bhatti, M. A. Hanif and R. Nadeem, *J. Hazard. Mater.*, 2009, **161**, 941-947.
50. M. A. Hanif, R. Nadeem, H. N. Bhatti, N. R. Ahmad and T. M. Ansari, *J. Hazard. Mater.*, 2007, **139**, 345-355.
51. I. Langmuir, *J. Am. Chem. Soc.*, 1918, **40**, 1361-1403.
52. R. Djeribi and O. Hamdaoui, *Desalination*, 2008, **225**, 95-112.
53. H. R. Yuan, T. Lu, H. Y. Huang, D. D. Zhao, N. Kobayashi and Y. Chen, *J. Anal. Appl. Pyrol.*, 2015, **112**, 284-289.
54. F.-C. Wu, R.-L. Tseng, S.-C. Huang and R.-S. Juang, *Chem. Eng. J.*, 2009, **151**, 1-9.

55. A. Y. Dursun, *Biochem. Eng. J.*, 2006, **28**, 187-195.
56. Y. S. Ho and G. McKay, *Water. Res.*, 2000, **34**, 735-742.
57. J. Febrianto, A. N. Kosasih, J. Sunarso, Y. H. Ju, N. Indraswati and S. Ismadji, *J. Hazard. Mater.*, 2009, **162**, 616-645.
58. M. I. Kandah, *Sep. Purif. Technol.*, 2004, **35**, 61-70.
59. T.-t. Li, Y.-g. Liu, Q.-q. Peng, X.-j. Hu, T. Liao, H. Wang and M. Lu, *Chem. Eng. J.*, 2013, **214**, 189-197.
60. S. Malamis and E. Katsou, *J. Hazard. Mater.*, 2013, **252**, 428-461.
61. Q.-S. Liu, T. Zheng, P. Wang, J.-P. Jiang and N. Li, *Chem. Eng. J.*, 2010, **157**, 348-356.
62. X. W. Ang, V. S. Sethu, J. M. Andresen and M. Sivakumar, *Clean Technologies and Environmental Policy*, 2013, **15**, 401-407.
63. M. Fomina and G. M. Gadd, *Bioresour. Technol.*, 2014, **160**, 3-14.
64. Y. Xiong, H. Wang, Z. Lou, W. Shan, Z. Xing, G. Deng, D. Wu, D. Fang and B. K. Biswas, *J. Hazard. Mater.*, 2011, **186**, 1855-1861.

The table of contents entry

Maximum adsorption capacity of perrhenate on ASBC is 14.6 $mg \cdot g^{-1}$ at pH 1.0, temperature 308K and initial concentration 100 $mg \cdot L^{-1}$.